Australian Government

Geoscience Australia

Technical Report

Cloud Shadow Algorithm

By Josh Sixsmith

TABLE OF CONTENTS

1.0 Introduction....4
2.0 Methodology....4
2.1 Background....4
2.2 Current method....5
2.2.1 Geometric calculations....5
2.2.2 Spectral tests....9
2.2.3 Pixel weights....9
2.2.4 Thresholding and region growing....10
3.0 Results....11
3.1 Geometric calculations....11
3.1.1 Cloud height estimation....11
3.1.2 Cloud shadow projection accuracy....14
3.2 Region Growing....15
3.3 Pixel weights....23
3.4 Processing times....24
4.0 Conclusion....24
5.0 Future Actions....25
6.0 References....27
7.0 Appendix A....28
8.0 Glossary....29

LIST OF FIGURES

Figure 1 Geometric formulation of cloud shadow....6
Figure 2 The complex plane....8
Figure 3 3D cloud model....11
Figure 4 3D cloud model....12
Figure 5 3D cloud model....12
Figure 6 Projected cloud pixels....13
Figure 7 A zoomed subset of Figure 6....13
Figure 8 Projected cloud pixels with cloud pixels removed....13
Figure 9 False colour (4,3,2 RGB) image of clouds....14
Figure 10 Clouds projected using 3 different lapse rates....15
Figure 11 Inaccurate cloud projection....15
Figure 12 False colour image (4,3,2 RGB) depicting cloud shadow....16
Figure 13 Cloud shadow mask resulting from region growing....16
Figure 14 False colour image (4,3,2 RGB)....17
Figure 15 Cloud shadow mask of Figure 14....17
Figure 16 False colour image (4,3,2 RGB)....18
Figure 17 Cloud shadow mask of Figure 16....18
Figure 18 False colour image (4,3,2 RGB)....19
Figure 19 Cloud shadow mask of Figure 18....19
Figure 20 False colour image (4,3,2 RGB) depicting cloud and water....20
Figure 21 Cloud shadow mask of Figure 20 showing the grown water body....20
Figure 22 False colour image (4,3,2 RGB) depicting cloud and water....21
Figure 23 Cloud shadow mask of Figure 22 depicting slight water fragmentation....21
Figure 24 False colour image (4,3,2 RGB) depicting cloud and water....22
Figure 25 Cloud shadow mask of Figure 24 depicting water fragmentation....22

Figure 26 False colour image (4,3,2 RGB) depicting cloud shadow and topographic shadow 23
Figure 27 Cloud shadow mask of Figure 26 23
Figure 28 Various spectral curves depicting the high reflectance of shadow over a soil target 24

1.0 Introduction

Like cloud, cloud shadow can also be considered a type image contaminant, as the underlying surface spectral characteristics are not truly represented. Visually and spectrally, dark cloud shadow can exhibit spectral properties similar to that of water, whereas lighter cloud shadow can look spectrally similar to darker vegetation (Luo *et al* 2008).

The basic premise that cloud shadow is a dark target. However, shadow over a bright target can result in a 'brighter' shadow. For instance, shadow over bright soil can in some instances be spectrally brighter than everything else, except for non-shadowed soil.

Various methods have been suggested and investigate as how best to identify cloud shadow. Such methods include:

- Manual digitisation
- Spectral tests
- Geometric

The method discussed in this report uses a combination of spectral tests and geometric calculations, followed by an implementation of a region growing algorithm.

2.0 Methodology

2.1 Background

The general assumption is that a shadow is dark. But how dark is that shadow? The thickness of the cloud and the type of land cover the shadow has obfuscated will dictate the brightness. For example if shadow is covering what normally would be a bright target. The brightness value of that shadowed target will be darker, but it will still be much brighter than that of a shadow over a dark target. The choice of band will also dictate of bright a normal target will be. For example dense healthy vegetation can be bright in band 4, but dark in band 5 due to leaf water content.

Irish (et al 2006) suggested 3 methods for detecting cloud shadow. The first is spectral based but could lead to the highest omission errors, likely due to the characteristics mentioned above by Amin (et al 2011) and Luo (et al 2008). The second approach is geometric and uses the thermal band to predict the height of the identified clouds. The sun's azimuth and elevation angles are then used to calculate the location of the shadow. The third and final approach assumes the highest possible height of the cloud, by which a projected area, large enough to cover all possible shadowed pixels, is created.

Choi and Bindschadler (2004) used spectral thresholds of bands 3 and 4 stating that shadow is brighter than water and darker than both cloud and

snow. However they also mention that land surfaces in a large mountains shadow could fall within the threshold limits. To aid in cloud shadow detection they employed a technique similar to a geometric prediction, and that a cloud shadow was classified only if a matching cloud could be found.

Anders *et al* (2011), Huang *et al* (2010), and Martinuzzi *et al* (2007) all used the geometric approach to predict cloud shadow locations. However their methods for creating the shadow mask differed. Anders populated the shadow mask by extending each shadow pixel one pixel towards its parent cloud. Huang's method was similar to that used by Luo *et al* (2008) which used the geometric technique in order to predict where shadow might be. Following the predictions, bands 4 and 5 (near-infrared and shortwave infrared respectively) were used to find dark pixels within the vicinity of the prediction. Huang reported high degrees of success with this approach yielding accuracies around 90%. Martinuzzi used a manual method of identifying a feature within a cloud as well as its shadow. This distance was assumed constant over the region. The cloud is then projected by the distance offset and a 10 pixel buffer applied. Within the projected and buffered region, brightness values within band 4 are used differentiate shadow from non-shadow.

2.2 Current method

The approach taken for this report included a combination of spectral tests, geometric calculations and finally a form of region growing via thresholds. The goal of this method was to keep it relatively simple, general enough to work for most regions, and time efficient for the bulk processing of the thousands of images located in Geoscience Australia's Landsat archive. Like ACCA (Automated Cloud Cover Assessment) developed by Irish, the cloud shadow algorithm is dependent upon a thermal band in order to estimate cloud height.

2.2.1 Geometric calculations

In order for any geometric calculations to take place, pixels with cloud must first be identified. Calculating cloud shadow locations can be determined using trigonometry. The following figure (Figure 1) demonstrates the relative idea.

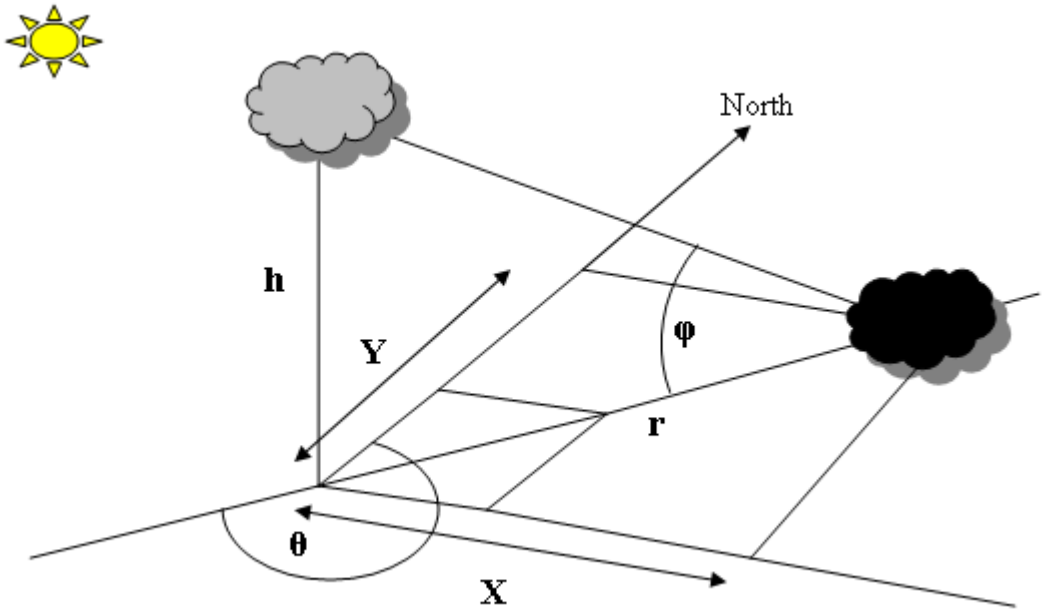

Figure 1 Geometric formulation of cloud shadow

The projected cloud distance 'r' is given by Equation 1.

Equation 1

$$r = \frac{h}{\tan(\varphi)}$$

Where:

r is the projected cloud shadow distance in metres

h is the cloud base height in metres

φ is the solar elevation angle (assumed constant over the entire image)

The cloud height (h) in metres is calculated using environmental lapse rates. Clouds are formed when rising parcels of air become saturated with water vapour. The temperature of such air parcels will fall as it rises. This decrease in temperature is defined as a lapse rate. Wikipedia describes two main types of lapse rates; environmental and adiabatic. Adiabatic comprises of a dry adiabatic lapse rate of approximately 9.8^{o}C/km and a wet adiabatic lapse rate of about 5^{o}C/km. Environmental lapse rates vary with time and location. The International Civil Aviation Organization defines a standard as 6.49^{o}C/km. For this study a value of 6.4^{o}C/km was used (similar to that used by Huang).
To estimate the cloud height, the following formula is used.

Equation 2 Cloud height estimation

$$h = \frac{(a-c)}{ELR}$$

Where:

h is cloud height in metres

a is surface air temperature
c is cloud temperature
ELR is the Environmental Lapse Rate

The mean of non-cloud areas was used to determine the surface temperature. In order to minimise disturbances in surface temperature, water and non-vegetated areas, were excluded using an NDVI value of greater than 0.5.

The solar elevation angle from Equation 1, is retrieved from the satellite header file and is assumed constant over the entire image array.

The distance from a cloud pixel, known as the origin, only gives one part of the picture. In order to retrieve a projected pixels location, in terms of an x and y co-ordinate, two methods are used for different cases based on the current image projection.

The first method is used for imagery that is in a metres projected space and is based around complex number theory in order to extract the x and y distance/location from the origin (cloud pixel) and is used for images with a projection reference system that is based on metres, for example UTM (Universal Transverse Mercator). While the second uses trigonometric calculations based on great circles, and is used for images in a latitude/longitude (geographic) reference system.

In the complex number plane, points expressed in polar form can be converted to a Cartesian co-ordinate based on the following formula:

Equation 3

$$x = r \times \cos(\theta)$$
$$y = r \times \sin(\theta)$$

Where:
x is the x-coordinate in the Cartesian plane (real part of the complex plane)
y is the y-coordinate in the Cartesian plane (imaginary part of the complex plane)
θ is the solar azimuthal angle (assumed constant over the entire image)
r is the projected cloud shadow distance from the origin

Figure 2 (below) depicts the complex plane.

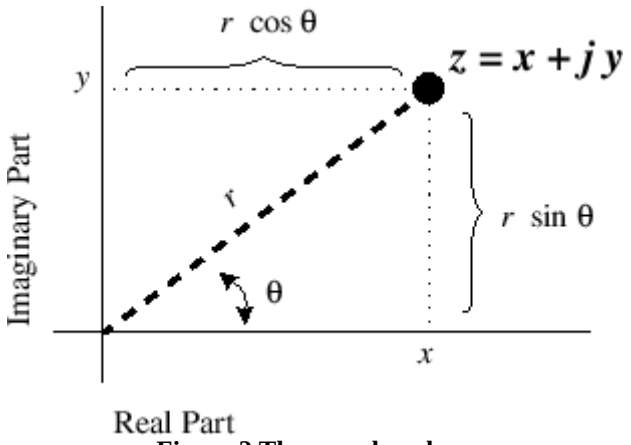

Figure 2 The complex plane

(Source: https://ccrma.stanford.edu/~jos/st/Complex_Plane.html)

The second method is based on great circles, and is used for un-projected imagery i.e. measured in degrees of latitude and longitude. The method of great circles uses spherical geometry to either calculate a distance between two points, or in our case given a starting point, distance and bearing, calculate a second location.
The equations for calculating the location in latitude and longitude are given in Equation 4 and Equation 5 below.

Equation 4

$$lat_2 = \arcsin\left(\sin(lat_1)\times\cos\left(\frac{d}{R}\right)+\cos(lat_1)\times\sin\left(\frac{d}{R}\right)\times\cos(\theta)\right)$$

Equation 5

$$lon_2 = lon_1 + \arctan 2\left(\sin(\theta)\times\sin\left(\frac{d}{R}\right)\times\cos(lat_1), \cos\left(\frac{d}{R}\right)-\sin(lat_1)\times\sin(lat_2)\right)$$

Where:

- Lat_2 is the latitude of the projected cloud pixel
- Lon_2 is the longitude of the projected cloud pixel
- d is the projected cloud shadow distance
- R is the earth's radius
- θ is the solar azimuth angle (assumed constant over the entire image)

(Source: http://www.movable-type.co.uk/scripts/latlong.html)

The earth's radius can vary between datum's that are created from different spheroids. As such, the value of R in Equation 4 is determined from the image's projection information stored in the header.

2.2.2 Spectral tests

Once the cloud pixels have been projected, a series of spectral tests are applied in order to remove those pixels that are either still located in the cloud, or have not projected cleanly to a 'shadowy object'.

Reasons for such unclean projections can occur from a variety of different factors. Differing surface temperatures across the image, which itself can be influenced by topography. Sensor saturation and atmospheric effects, as well as incorrectly classified cloud pixels can all lead to inaccurate projections.

The spectral response for cloud shadow is relatively low, and in some cases for thick cloud, can look very similar to water. In fact cloud shadow pixels can take on a wide variety of spectral responses, depending on what land cover they have obfuscated.

In order to retain some of the more definite shadow pixels, a green band threshold is set relatively low at 0.045% reflectance, which will also remove some pixels representing deep water. The NIR band is used as the other spectral elimination test, and is set at 0.12% reflectance. While this seems high compared to the green test, the aim was retain more of the pixels that had fallen on strong healthy vegetation.

2.2.3 Pixel weights

An array of individual pixel weights is created and used in the development of a weighted band combination.

Firstly the pixels are weighted via the slope of the spectral curve. In deriving the slope, the horizontal distance is defined as the band number position. While this may not be a true slope in the sense that horizontal distance would normally be described by the wavelength, but it still achieves the desired result for our purposes. The purpose of weighting pixels was to eliminate some confusion/misclassifications that between different land covers and their shadowed equivalents. For example shadow on dense vegetation in some instances appears identical to fallowed land, especially in band 4.

Every pixel starts out with a weight of one. Next a weight of 1 is added to those pixels that have a slope greater than or equal to 0.1 between bands 3 and 4. This is to eliminate some of the darker vegetation as described by Luo *et al* 2008. Next, pixels with a slope greater than or equal to 0.05 between bands 4 and 5 have a weight increase of 1. This is to discriminate between shadows of fallowed land, and unshadowed fallowed land with shadowed vegetation. The final slope is made from band 4 through 7. Pixels that are slightly greater than the horizontal (0.01) have their weights added by one. This last slope is used to eliminate more of the fallowed land as well as soils and dry grasses. Additional slopes could be used to aid in discriminating other spectrally similar features, and whether to increase or decrease weights. But at this stage we have settled with 3. Additional testing on processed

images will no doubt find cases where other weighting systems will need to be defined for differing land covers.

The final weighting is assigned to water pixels, and set quite high with a value of 9. This is because deep water and less turbid water, is generally low in all bands. So when computing a weighted summation, unless water is scaled high using a high weighting, it will generally still be within valid thresholds.

The water mask is given in given in Equation 6 below:

Equation 6

$$Water = (NDVI < 0.1) \& (b5 < 0.05)$$

The equation for the weighted sum is given in Equation 7 (below). Note that bands 5 and 7 the weights are doubled in order to further differentiate shadowed vegetation and fallowed land.

Equation 7

$$W\_sum = weights \times (b1 + b2 + b3 + b4) + 2 \times weights \times (b5 + b7)$$

2.2.4 Thresholding and region growing

The next stage implements a basic form of segmentation via thresholding, whereby contiguous segments are labelled and matched to the projected pixels. This in effect gives a form of region growing.
The thresholds are derived from a weighted sum of bands 1-5 and 7. The reason for using a combination of all bands; is that no single band can effectively be used to describe what a shadow is. The general assumption is that a shadow is dark. But how dark is that shadow? The thickness of the cloud and the type of land cover the shadow has obfuscated will dictate the brightness. For example if shadow is covering what normally would be a bright target. The brightness value of that shadowed target will be darker, but it will still be much brighter than that of a shadow over a dark target. The choice of band will also dictate of bright a normal target will be. For example dense healthy vegetation can be bright in band 4, but dark in band 5 due to leaf water content.

In deriving the thresholds that were to be used for growing shadowed locations, an upper threshold of 0.9 was used to partition the weighted sum into 10 bins. This was to create statistically localised regions and grow each bin separately. Each bin was grown by 2.5 standard deviations, thus giving a relaxed or even fuzzy threshold for the upper and lower limits. However, growing each bin added to the processing time, and we opted to go for a single growing threshold. The statistics from each bin are still calculated, where the relaxed/fuzzy threshold of the final bin is used as the upper limit for thresholding.

After the threshold has been applied, the result is then labelled into contiguous segments. The projected cloud pixels that have survived the

spectral tests are then used to identify which segments are to be used as the cloud shadow mask.

Finally the identified cloud shadow segments have a majority filter applied twice in order to fill holes and remove isolated pixels.

3.0 Results

Results so far have shown to be quite successful for a large number of scenes, covering a number of different land covers.

A complete list of the scenes used for testing the cloud shadow algorithm, are given in **Error! Reference source not found.**.

3.1 Geometric calculations

The method of projecting the cloud to a probable cloud shadow location has shown that the method doesn't perfectly map to a shadow location. This to a large extent was expected due to the nature of approximating cloud height with standard lapse rates. Lapse rates can vary from scene to scene, as well as within a standard scene depending on the current weather and atmospheric conditions. The calculations for estimating a clouds temperature are based on 'at sensor measurements', and don't take into effect any atmospheric effects. Nevertheless, the method has thus far been adequate in predicting a cloud shadows location, from which the region growing method uses successfully projected pixels to grow the shadowed object.

3.1.1 Cloud height estimation

The following figures (Figure 3 through Figure 5) depict 3D visualisations of detected cloud with a small sample of pixels projected to probable shadow locations. The underlying rasters were re-sampled to a lower resolution in order to reduce the computer's load when visualising the results.

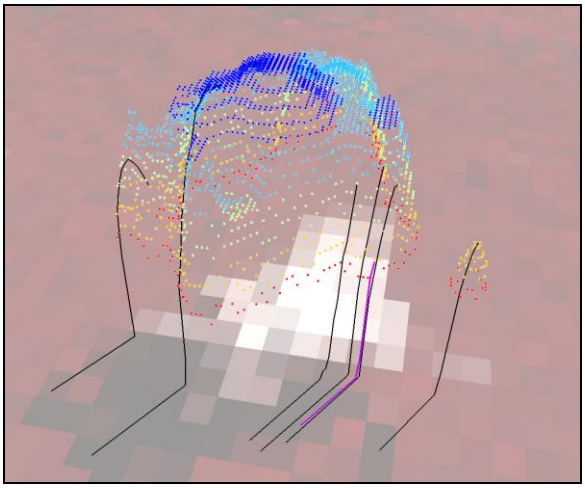

Figure 3 3D cloud model

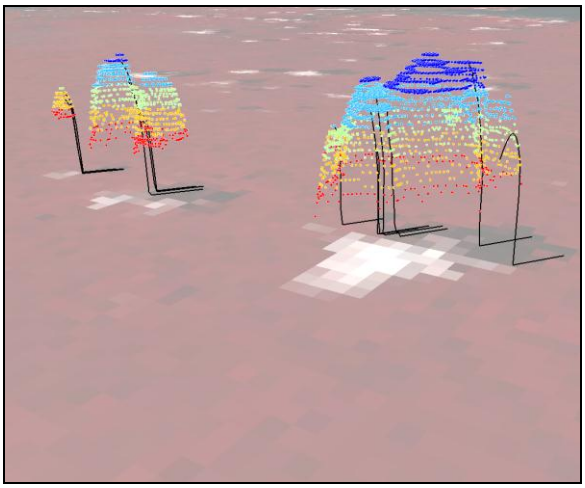

Figure 4 3D cloud model

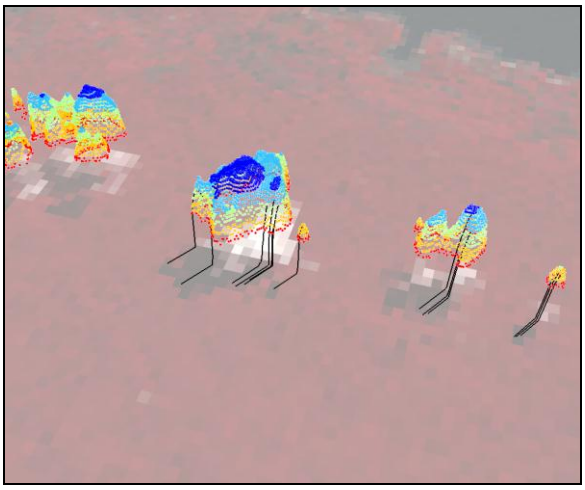

Figure 5 3D cloud model

It was found that pixels from the centre of a cloud mapped to a shadow location more cleanly than those from a cloud's edge. This could most likely be due to a stronger reflected signal, thereby giving a more accurate temperature reading.

Figure 6 (below) shows the projected cloud (in white). A topographic look is clearly seen, where steeper changes in cloud height have gaps (black areas) in the projection, while constant/similar height values in the cloud have projected smoothly and create a white coloured fill.

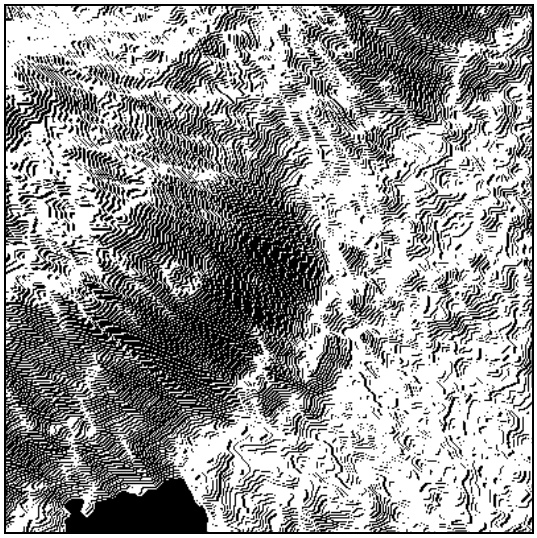

Figure 6 Projected cloud pixels

Figure 7 (below) is a zoomed subset of Figure 6 (above) that depicts the changes in cloud height.

Figure 7 A zoomed subset of Figure 6

In order to map the cloud shadow, the co-existence of cloud and shadow has to be identified and removed. Figure 8 (below) shows the result of removing co-existing cloud and cloud shadow (projected cloud) pixels.

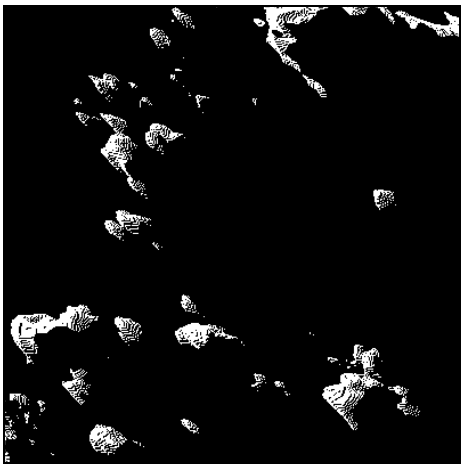

Figure 8 Projected cloud pixels with cloud pixels removed

3.1.2 Cloud shadow projection accuracy

The method for detecting cloud shadow in this algorithm didn't require absolute accuracy in determining a shadows location. The idea was to project the cloud pixels to a location where the corresponding cloud shadow was most likely to be found. The region growing part would then take care of the rest. Due to the high variability in determining a clouds height, the projected shadow location isn't guaranteed.

An update to the current projection method involves projecting cloudy pixels using three different lapse rates; saturated (4.8), normal (6.4) and dry (9.8). By projecting clouds using three different lapse rates, the algorithm has the potential to capture the height variations occurring within a cloud, and clouds across the scene that have different saturation states. A major drawback is the potential to grow un-shadowed areas that fall within valid threshold ranges.

The following 2 figures (Figure 9 and Figure 10) show a false colour image (bands 4, 3, 2 RGB) and the associated cloud projection using 3 different lapse rates. The green represents clouds projected using a saturated lapse rate; the blue represents clouds projected using a normal (or standard lapse rate); the yellow represents clouds projected using a dry lapse rate.

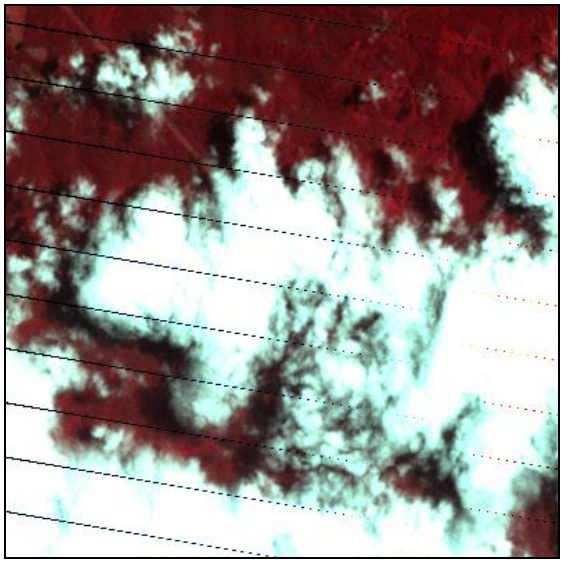

Figure 9 False colour (4,3,2 RGB) image of clouds

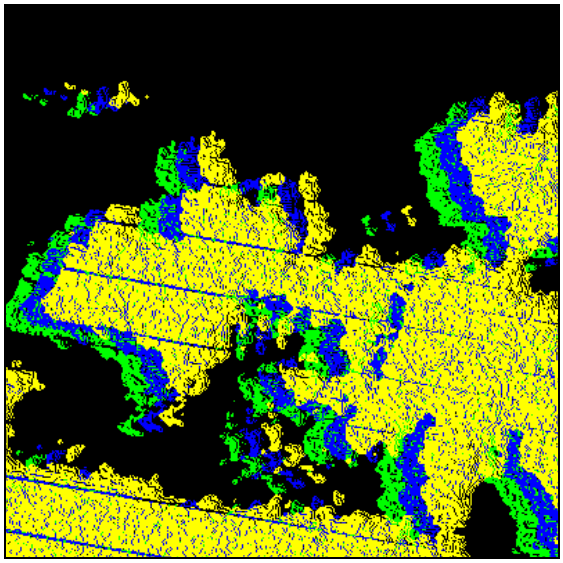

Figure 10 Clouds projected using 3 different lapse rates

There have been cases within a single scene where the standard lapse rate was suitable for predicting the shadow location for one cloud, while in other parts of the scene either the dry or the wet lapse rate was found to be more suitable. Figure 11 (below) presents a case when neither the dry, wet nor the standard lapse rate was suitable for predicting the shadow location. This resulted in that cloud's shadow not being added to the mask.

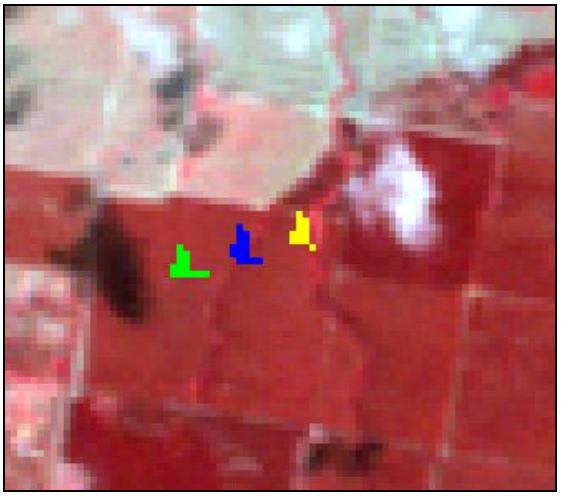

Figure 11 Inaccurate cloud projection

The most probable cause for the cloud projection undershoot, is that the cloud itself is quite small, thus an accurate temperature reading is unlikely.

3.2 Region Growing

For most practical purposes, the method of region growing has worked quite well. Most areas under cloud shadow have been identified and subsequently masked. Some shadowed areas have been missed which could be due to an unsuccessful cloud projection, or the pixel values for the shadowed area are higher than the threshold.

Figure 12 (below) shows a false colour image (bands 4, 3, 2 as RGB). One can see that cloud shadows are slightly larger than their respective clouds. One must remember that a cloud is a volume, whereby a taller cloud, has the potential to cast a larger shadow than a cloud with a larger area in the xy (planar) dimension.

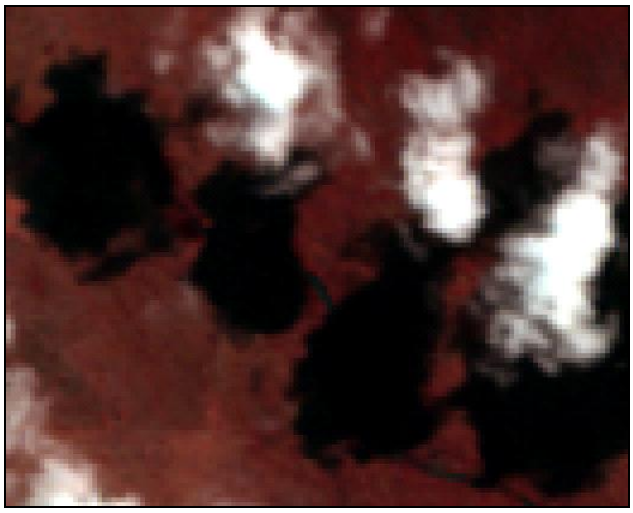

Figure 12 False colour image (4,3,2 RGB) depicting cloud shadow

Figure 13 (below) is the resulting cloud shadow mask using the region growing method.

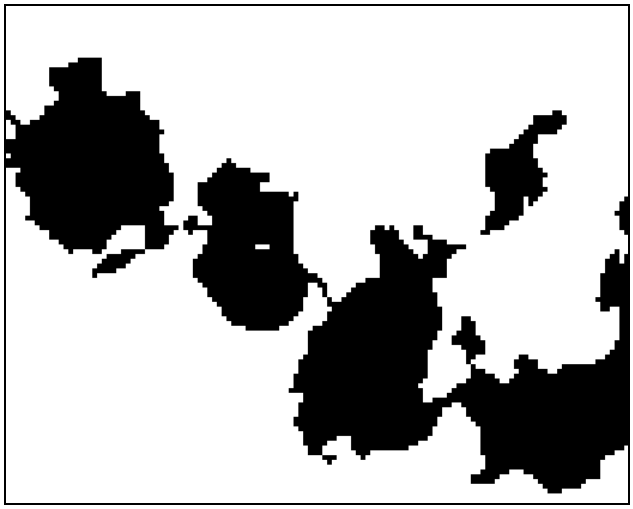

Figure 13 Cloud shadow mask resulting from region growing

Figure 14 through Figure 17 (below) depict the false colour images (bands 4, 3, 2 as RGB) and their associated cloud shadow masks.

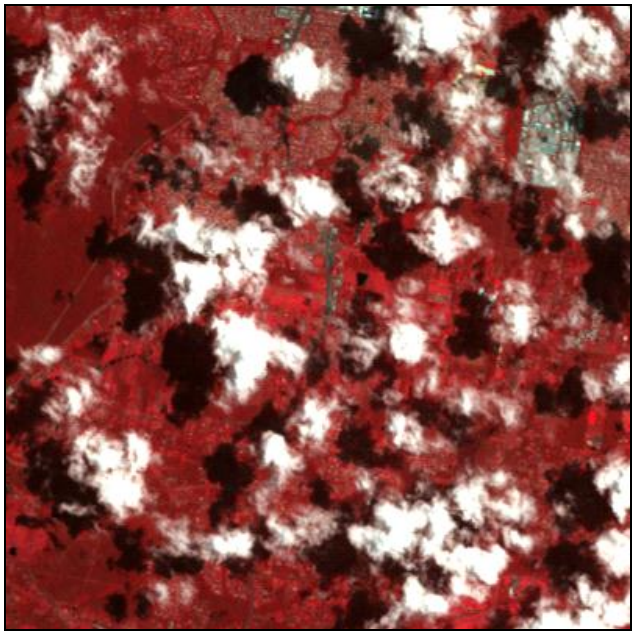

Figure 14 False colour image (4,3,2 RGB)

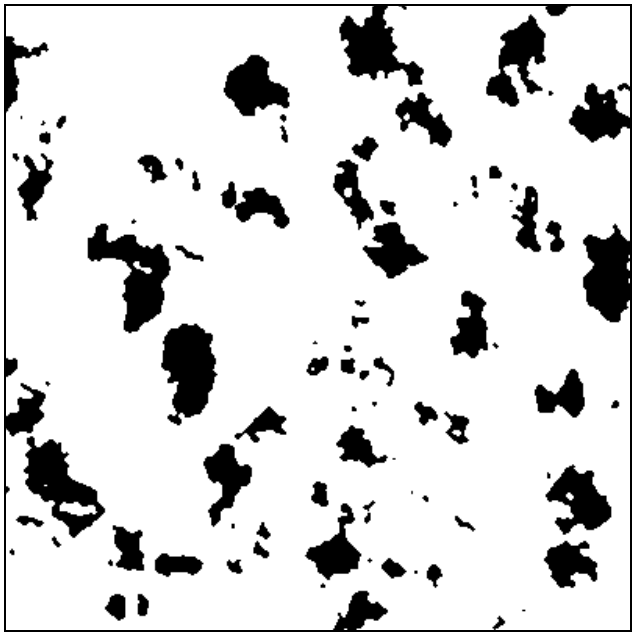

Figure 15 Cloud shadow mask of Figure 14

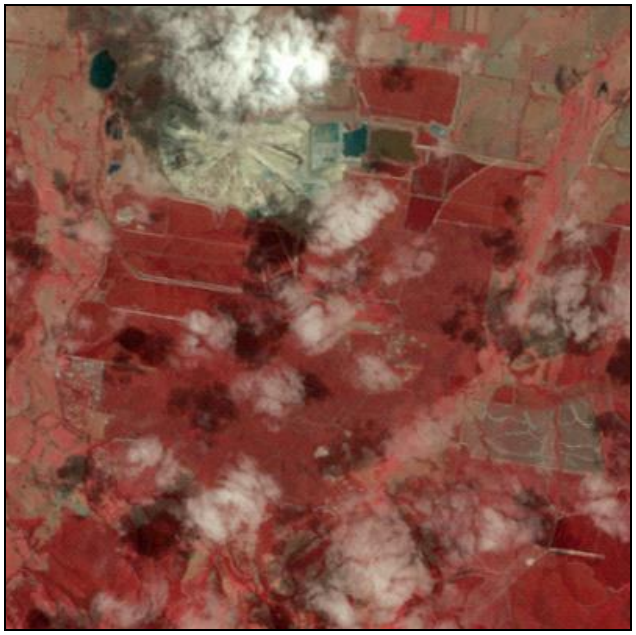

Figure 16 False colour image (4,3,2 RGB)

The cloud shadow masks appear to have captured the cloud shadow quite well. The edges of the cloud shadow are also captured thereby minimising the need for pixel buffering/dilation.

Figure 17 Cloud shadow mask of Figure 16

The following figures (Figure 18 and Figure 19) present a case where the cloud shadow is not as dark spectrally, as well as intermixed with lots of smaller thin clouds.

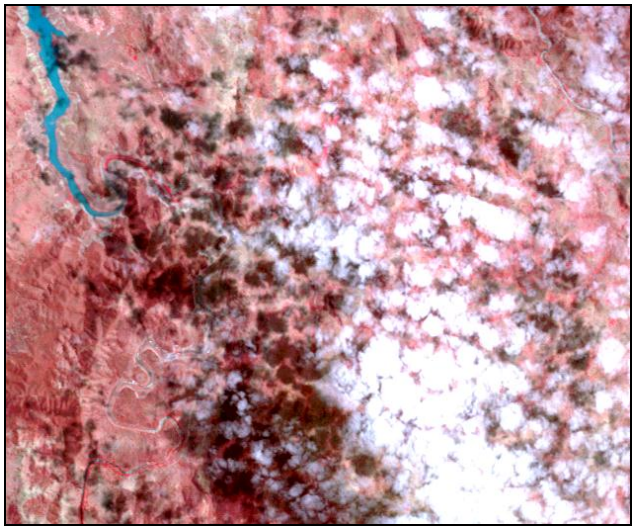

Figure 18 False colour image (4,3,2 RGB)

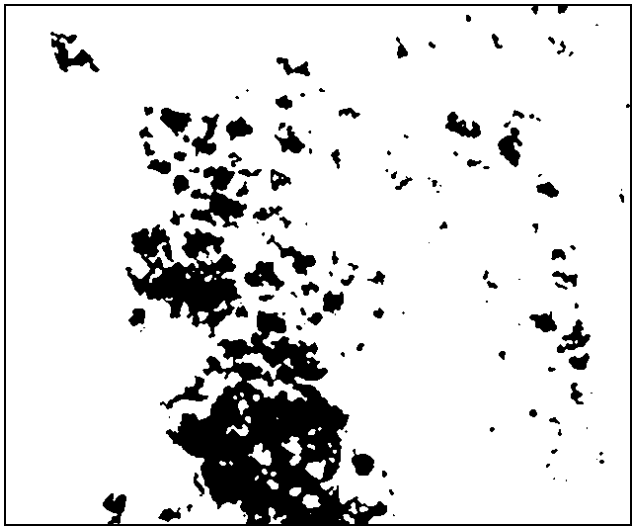

Figure 19 Cloud shadow mask of Figure 18

However, the region growing method does suffer from 'over-grown' regions. This is more noticeable in scenes with water bodies. While a water mask is used to identify water, not all water bodies will be flagged as water in the mask. Some shadowed areas may in fact be identified as water in the water mask. This is due to water and shadow can exhibit very similar spectral properties. Not all water bodies get classified as shadow. In Figure 18 (above) the top left hand corner of the image presents such a case where the shadow is cast onto the water, but the water body has not grown. The growing of water bodies tends to only occur with the spectrally darker water bodies.

Figure 20 and Figure 21 (below) depict such a case where a small section of cloud shadow has grown the entire water body.

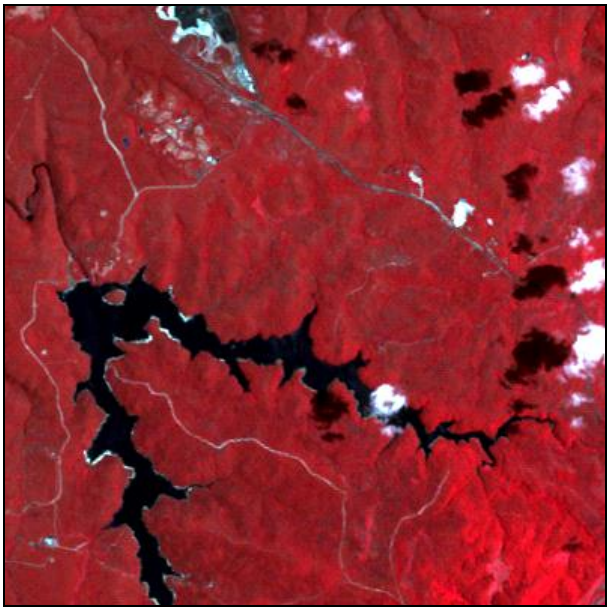

Figure 20 False colour image (4,3,2 RGB) depicting cloud and water

Figure 21 Cloud shadow mask of Figure 20 showing the grown water body

In some cases a water body may become fragmented once thresholds are applied, as some pixels will be higher than the threshold, while some pixels will be lower than the threshold. This fragmenting can result in smaller grown segments that may not contain a projected cloud pixel and therefore not included in the final cloud shadow mask.

Figure 22 (below) shows a false colour image (bands 4, 3, 2 as RGB) depicting similarities between cloud shadow and water. Even for the human eye it is difficult to distinguish between water and shadow, without using the clouds as a guide.

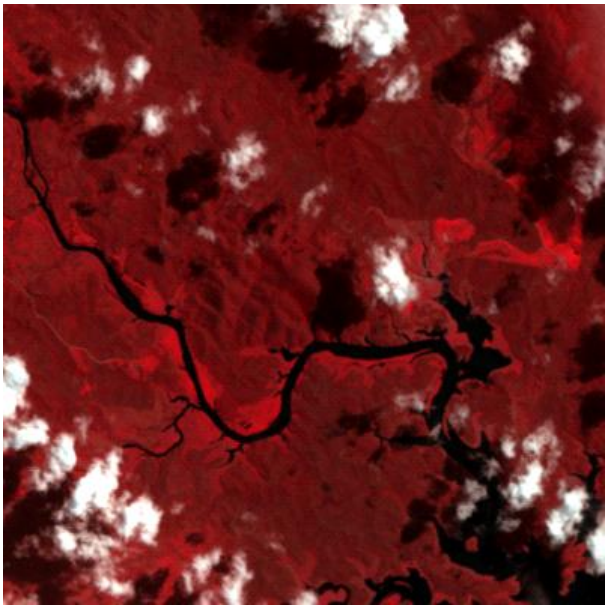

Figure 22 False colour image (4,3,2 RGB) depicting cloud and water

Figure 23 (below) shows the resulting cloud shadow mask with the water considered as an 'over-grown' region. Some fragmenting has occurred of water bodies has occurred in the bottom right hand corner of the image, but not enough to make discontinuous segments that would stop the 'growing' effect.

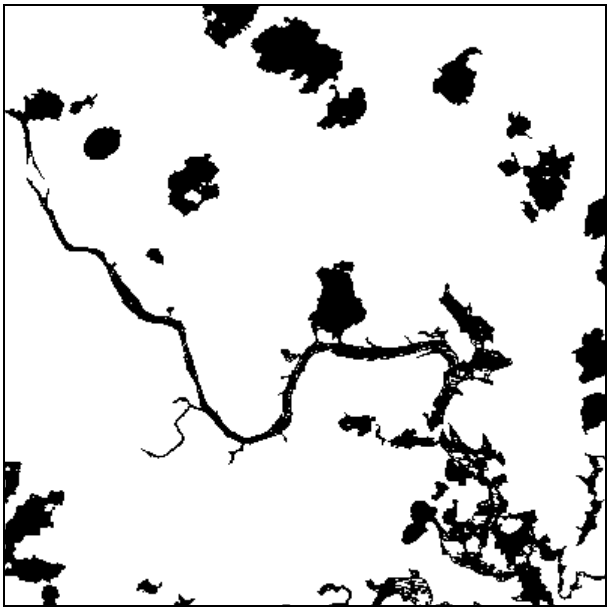

Figure 23 Cloud shadow mask of Figure 22 depicting slight water fragmentation

Figure 24 and Figure 25 (below) shows a false colour image (bands 4, 3, 2 as RGB) and the associated cloud shadow mask. Here the fragmenting of the water bodies has had slightly better success (in the centre of the image) compared to Figure 23, with shadow on water being masked while leaving the neighbouring unshadowed water pixels.

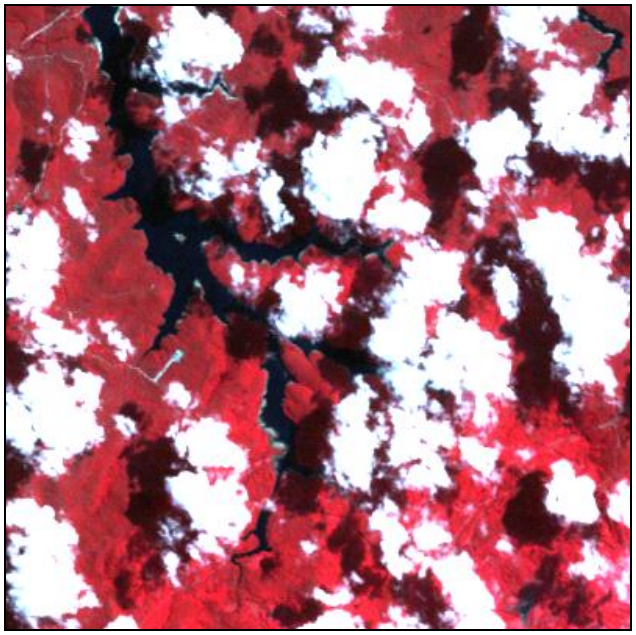

Figure 24 False colour image (4,3,2 RGB) depicting cloud and water

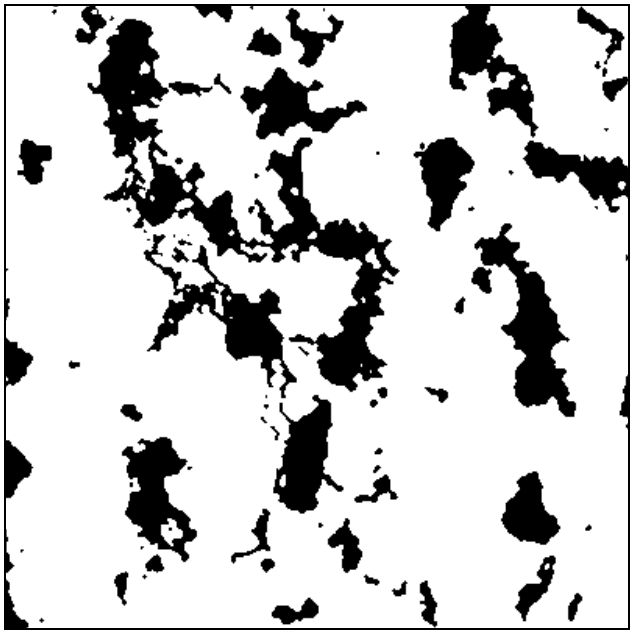

Figure 25 Cloud shadow mask of Figure 24 depicting water fragmentation

Other cases of 'over-grown' regions occur in areas subject to topographical shadow. In these instances they are both a shadowed object and difficult to distinguish between the two, unless there are no clouds. The solar position, shape of the landscape and the spectral response of the underlying terrain dictate how illuminated the underlying terrain will be; much in the same way that the thickness of the cloud is an important factor in determining how dark the terrain will appear.

Figure 26 (below) is a false colour image (bands 4, 3, 2 as RGB) depicting cloud shadow falling in a region containing topographical shadow.

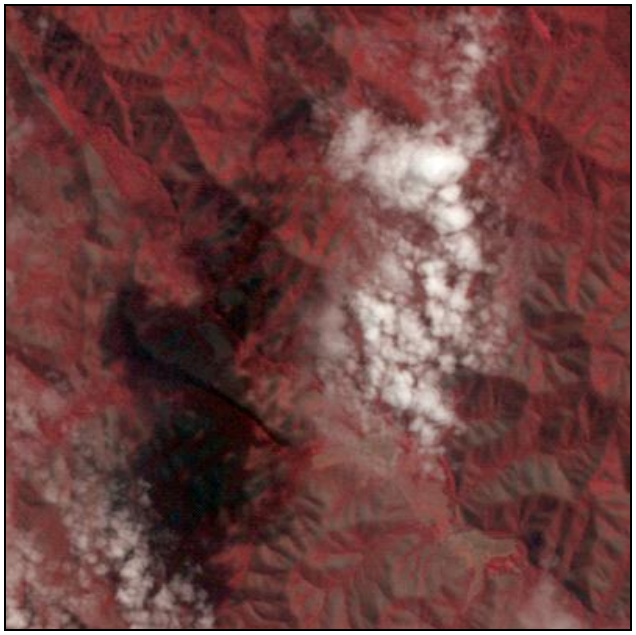

Figure 26 False colour image (4,3,2 RGB) depicting cloud shadow and topographic shadow

Figure 27 (below) shows the resulting cloud shadow mask of Figure 26. One can see in the top left hand corner of the image where the 'grown' region includes topographic shadow.

Figure 27 Cloud shadow mask of Figure 26

3.3 Pixel weights

The weighting system has appeared to work well for most shadowed regions. As discussed above in section 3.2, darker water bodies tend to fall within the thresholds derived from the weighted summation. However, shadows over bright soils tend to fall outside the threshold range. The following figure (Figure 28) depicts spectral curves of various targets that are in shadow and normal lit conditions.

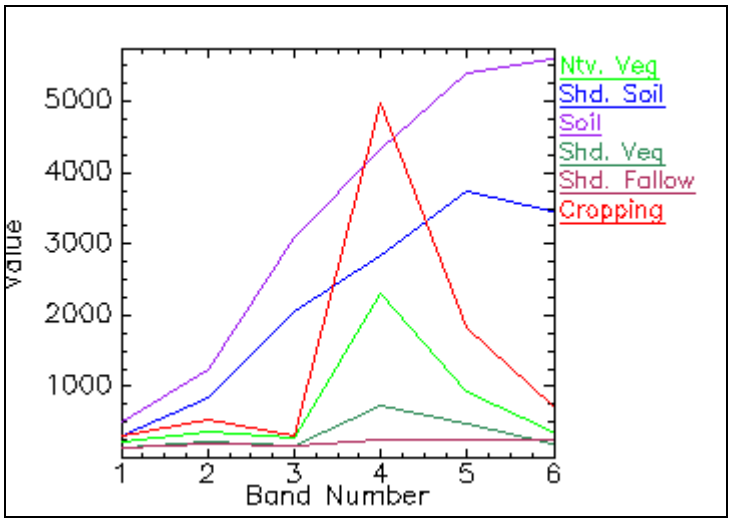

Figure 28 Various spectral curves depicting the high reflectance of shadow over a soil target

As one can see, using a weighted summation of the bands is going to eliminate, quite early during the addition calculation, shadowed soil targets.

3.4 Processing times

One of the main constraints associated with the Pixel Quality algorithms developed for the Unlocking the Landsat Archive project at Geoscience Australia, is processing time. With more than 100000 Landsat scenes from the years 2000 to 2010, it was deemed undesirable to have a flagging system that would take too long to process a single scene.
Currently, the cloud shadow algorithm takes roughly 1min to process a single Landsat scene comprising of approximately 9000 by 9000 pixels. Some scenes run as quick as 35secs while others take up to 1min 30secs. This is deemed to be quite suitable, but there is still room for improvement. A large bulk of the time is spent identifying which grown regions are linked to projected cloud pixels.

4.0 Conclusion

While the method presented here for the detection and masking of cloud shadow is far from perfect, it does however, provide a reasonably good method of masking cloud shadow. Finding literature that deals with the identification and masking of cloud shadow of medium resolution multi-spectral imagery is fairly sparse. Most articles agree that it is a very challenging task. The main challenge associated with cloud shadow masking is that shadows can take on a range of brightness values. How dark a target will be, depends on the thickness of the cloud that is obscuring the target, and how naturally reflective the target is under normal conditions.

The current method of projecting the cloudy pixels as of yet doesn't appear to be faulty. The algorithm can cater for both projected (metres) and un-projected (latitude/longitude) systems. The accuracy of the projection is down to how accurate the algorithm can determine the height of a cloudy pixel.

A major issue identified with the current methodology is the growing of water bodies that weren't flagged by the water mask. A more suitable water mask could be utilised, however developing a more suitable water mask may result in lengthy developmental times for little improvement in the cloud shadow masking.

The flagging of pixels that are under shadow by topography rather than cloud is to a larger degree unsolvable using spectral methods. After all, both represent targets that are obfuscated by another target; whether that be terrain or cloud, it is still shadow. However, the flagging of topographically shadowed pixels can be solved using the method developed by Fuqin Li. The algorithm itself has been developed and a version for use within the pixel quality algorithm has been tested and may be released in a later version of pixel quality.

The weighted summation of the bands needs to be improved by either assigning new weights for features such as soil and water, or developing a different combined statistic.

5.0 Future Actions

In order to minimise the inclusion of water in the region growing algorithm, a method that halts the growing effect could be used. Grown pixels that are closer to projected cloudy pixels could be assigned higher (or lower) weights, similar to the interpolation method 'Inverse Distance Weighted'. However this assumes that the cloudy pixels have been projected accurately, which may not necessarily not the case. The method used in this process doesn't assume that the projected locations are correct; rather the current design is more akin to 'this is where shadow pixels are likely to be'.
(Update, tighter spectral constraints and improved mask has reduced the amount of water inclusions as well as topographic shadow.)

A follow-up segmentation process, potentially a histogram based segmentation method could be used to look for abnormalities in the grown pixels.

A reinvestigation into growing pixels via statistical bins, however a more efficient method of linking grown regions with projected pixels needs to be implemented. One such method would be a function similar to the histogram function present in IDL (Exelis Visual Information Solutions).
(Update, I have developed a histogram function that replicates IDL's using a combination of Python and FORTRAN. Times for identifying grown regions have been reduced quite significantly).

Develop a more accurate method of estimating the height of cloudy pixels, which in turn would increase the accuracy of the geometric projection.

Investigate the potential of using TOAR rather than NBAR. As NBAR is corrected for light scattering, using TOAR might provide better spectral separation with more diffuse light especially at the blue wavelength.

Incorporation of a DEM to aid in a more accurate estimation of cloud height.

6.0 References

Amin, R., Gould, R., Hou, W., Lee, Z., Arnone, R., 2011, Automated detection and removal of cloud shadows on HICO images, Proc. SPIE 8030, 803004, doid:10.1117/12.887761

Anders, K., Latifovic, R., Pouliot, D., 2011, A cloud detection algorithm for AATSR data, optimized for daytime observations in Canada, *Remote Sensing of Environment*, doi:10.1016/j.rse.2011.07.001

Bindschadler, R., Vornberger, P., Fleming, A., Fox, A., Mullins, J., Binnie, D., Paulsen, S.J., Granneman, B., Gorodetzky, D., 2008, *Remote Sensing of Environment*, Vol. 112, Iss. 12, pp. 4214-4226, doi:10.1016/j.rse.2008.07.006.

Choi, H., Bindschadler, R., 2004, Cloud detection in Landsat imagery of ice sheets using shadow matching technique and automatic normalized difference snow index threshold value decision, *Remote Sensing of Environment*, Vol. 91, pp.237-242, doi:10.1016/j.rse.2004.03.007.

Huang, C., Thomas, N., Goward, S.N., Masek, J.G., Zhu, Z., Townsend, J.R.G., Vogelmann, J.E., 2010, Automated masking of cloud and cloud shadow for forest change analysis using Landsat images. *International Journal of remote Sensing*, Vol. 31, No. 20, pp. 5449-5464.

Irish, R.R., Barker, J.L., Goward, S.N., Arvidson, T., 2006, Characterization of the Landsat-7 ETM+ Automated Cloud –Cover Assessment (ACCA) Algorithm, *Photogrammetric Engineering & Remote Sensing*, Vol. 72, No. 10, pp. 1179-1188.

Luo, Yi., Trishchenko, A.P., Khlopemkov, K.V., 2008, Developing clear-sky, cloud and cloud shadow mask for producing clear-sky composites at 250-meter spatial resolution for the seven MODIS land bands over Canada and North America, *Remote Sensing of Environment*, Vol 112, Issue 12, pp. 4167-4185.

Martinuzzi, S., Gould, W.A., Ramos Gonzalez, O.M., 2007, Creating cloud-free Landsat ETM+ data sets in tropical landscapes: Cloud and cloud-shadow removal, United States Department of Agriculture, Forest Service, General Technical Report IITF-GTR-32.

7.0 Appendix A

LS7_ETM_OTH_P51_GALPGS01-002_092_086_20050112
LS5_TM_OTH_P51_GALPGS01-002_092_086_20050120
LS7_ETM_OTH_P51_GALPGS01-002_106_072_20060102
LS7_ETM_OTH_P51_GALPGS01-002_092_086_20060115
LS5_TM_OTH_P51_GALPGS01-002_092_086_20060123
LS7_ETM_OTH_P51_GALPGS01-002_092_086_20070102
LS5_TM_OTH_P51_GALPGS01-002_092_086_20070126
LS5_TM_OTH_P51_GALPGS01-002_092_080_20070721
LS7_ETM_OTH_P51_GALPGS01-002_092_085_20080105
LS5_TM_OTH_P51_GALPGS01-002_092_086_20080113
LS7_ETM_OTH_P51_GALPGS01-002_092_086_20080121
LS5_TM_OTH_P51_GALPGS01-002_092_086_20080129
LS5_TM_OTH_P51_GALPGS01-002_091_076_20080310
LS5_TM_ OTH_P51_GALPGS01-002_091_077_20080310
LS5_TM_OTH_P51_GALPGS01-002_091_078_20080310
LS5_TM_OTH_P51_GALPGS01-002_091_079_20080310
LS5_TM_OTH_P51_GALPGS01-002_091_080_20080310
LS5_TM_OTH_P51_GALPGS01-002_091_081_20080310
LS5_TM_OTH_P51_GALPGS01-002_091_082_20080310
LS5_TM_OTH_P51_GALPGS01-002_091_083_20080310
LS5_TM_OTH_P51_GALPGS01-002_091_084_20080310
LS5_TM_OTH_P51_GALPGS01-002_091_085_20080310
LS5_TM_OTH_P51_GALPGS01-002_091_086_20080310
LS5_TM_OTH_P51_GALPGS01-002_091_087_20080310
LS7_ETM_OTH_P51_GALPGS01-002_092_086_20090107
LS5_TM_OTH_P51_GALPGS01-002_092_086_20090115
LS5_TM_OTH_P51_GALPGS01-002_090_084_20090117
LS7_ETM_OTH_P51_GALPGS01-002_092_086_20090123
LS5_TM_OTH_P51_GALPGS01-002_090_084_20090202
LS7_ETM_OTH_P51_GALPGS01-002_097_069_20090212
LS5_TM_OTH_P51_GALPGS01-002_090_084_20090306
LS7_ETM_OTH_P51_GALPGS01-002_091_081_20090609
LS7_ETM_OTH_P51_GALPGS01-002_113_065_20091111
LS7_ETM_OTH_P51_GALPGS01-002_093_087_20100102
LS7_ETM_OTH_P51_GALPGS01-002_093_088_20100102
LS7_ETM_OTH_P51_GALPGS01-002_100_078_20100103
LS7_ETM_OTH_P51_GALPGS01-002_092_086_20100110
LS7_ETM_OTH_P51_GALPGS01-002_092_081_20100110
LS5_TM_OTH_P51_GALPGS01-002_100_078_20100111
LS7_ETM_OTH_P51_GALPGS01-002_115_074_20100112
LS7_ETM_OTH_P51_GALPGS01-002_115_075_20100112
LS7_ETM_OTH_P51_GALPGS01-002_115_076_20100112
LS7_ETM_OTH_P51_GALPGS01-002_115_077_20100112
LS7_ETM_OTH_P51_GALPGS01-002_115_078_20100112
LS7_ETM_OTH_P51_GALPGS01-002_115_079_20100112
LS5_TM_OTH_P51_GALPGS01-002_096_070_20100115
LS5_TM_OTH_P51_GALPGS01-002_096_071_20100115
LS5_TM_OTH_P51_GALPGS01-002_096_072_20100115
LS5_TM_OTH_P51_GALPGS01-002_096_073_20100115
LS5_TM_OTH_P51_GALPGS01-002_096_074_20100115
LS5_TM_OTH_P51_GALPGS01-002_096_075_20100115
LS5_TM_OTH_P51_GALPGS01-002_096_076_20100115
LS5_TM_OTH_P51_GALPGS01-002_096_078_20100115
LS5_TM_OTH_P51_GALPGS01-002_096_080_20100115
LS5_TM_OTH_P51_GALPGS01-002_096_081_20100115
LS5_TM_OTH_P51_GALPGS01-002_096_082_20100115
LS5_TM_OTH_P51_GALPGS01-002_096_083_20100115
LS5_TM_OTH_P51_GALPGS01-002_096_084_20100115
LS5_TM_OTH_P51_GALPGS01-002_096_085_20100115
LS5_TM_OTH_P51_GALPGS01-002_096_086_20100115
LS7_ETM_OTH_P51_GALPGS01-002_095_083_20100116
LS7_ETM_OTH_P51_GALPGS01-002_091_077_20100119
LS7_ETM_OTH_P51_GALPGS01-002_100_078_20100119
LS7_ETM_OTH_P51_GALPGS01-002_095_082_20100116
LS5_TM_OTH_P51_GALPGS01-002_095_082_20100124
LS5_TM_OTH_P51_GALPGS01-002_095_083_20100124
LS7_ETM_OTH_P51_GALPGS01-002_092_083_20100126
LS7_ETM_OTH_P51_GALPGS01-002_092_086_20100126
LS7_ETM_OTH_P51_GALPGS01-002_115_066_20100128
LS7_ETM_OTH_P51_GALPGS01-002_115_075_20100128
LS7_ETM_OTH_P51_GALPGS01-002_115_076_20100128
LS7_ETM_OTH_P51_GALPGS01-002_115_077_20100128
LS7_ETM_OTH_P51_GALPGS01-002_115_078_20100128
LS7_ETM_OTH_P51_GALPGS01-002_115_079_20100128
LS7_ETM_OTH_P51_GALPGS01-002_095_082_20100201
LS7_ETM_OTH_P51_GALPGS01-002_095_083_20100201
LS5_TM_OTH_P51_GALPGS01-002_095_082_20100209
LS5_TM_OTH_P51_GALPGS01-002_095_083_20100209
LS5_TM_OTH_P51_GALPGS01-002_102_075_20100210
LS5_TM_OTH_P51_GALPGS01-002_109_066_20100211
LS5_TM_OTH_P51_GALPGS01-002_091_081_20100212
LS5_TM_OTH_P51_GALPGS01-002_105_078_20100215
LS7_ETM_OTH_P51_GALPGS01-002_104_069_20100216
LS5_TM_OTH_P51_GALPGS01-002_106_078_20100222
LS7_ETM_SYS_P31_GALPGS01-002_095_082_20100305
LS7_ETM_SYS_P31_GALPGS01-002_095_083_20100305
LS7_ETM_OTH_P51_GALPGS01-002_095_082_20100321
LS7_ETM_OTH_P51_GALPGS01-002_095_083_20100321
LS5_TM_SYS_P31_GALPGS01-002_095_082_20100329
LS5_TM_OTH_P51_GALPGS01-002_095_083_20100329
LS7_ETM_OTH_P51_GALPGS01-002_095_082_20100406
LS7_ETM_OTH_P51_GALPGS01-002_095_083_20100406
LS5_TM_OTH_P51_GALPGS01-002_095_082_20100430
LS5_TM_OTH_P51_GALPGS01-002_095_083_20100430
LS7_ETM_OTH_P51_GALPGS01-002_095_082_20100508
LS7_ETM_OTH_P51_GALPGS01-002_095_083_20100508
LS7_ETM_SYS_P31_GALPGS01-002_095_082_20100524
LS7_ETM_SYS_P31_GALPGS01-002_095_083_20100524
LS7_ETM_OTH_P51_GALPGS01-002_095_082_20100609
LS7_ETM_OTH_P51_GALPGS01-002_095_083_20100609
LS7_ETM_OTH_P51_GALPGS01-002_095_082_20100625
LS7_ETM_OTH_P51_GALPGS01-002_095_083_20100625
LS7_ETM_OTH_P51_GALPGS01-002_095_082_20100711
LS7_ETM_OTH_P51_GALPGS01-002_095_083_20100711
LS7_ETM_OTH_P51_GALPGS01-002_095_082_20100727
LS7_ETM_OTH_P51_GALPGS01-002_095_083_20100727
LS7_ETM_SYS_P31_GALPGS01-002_095_082_20100812
LS7_ETM_SYS_P31_GALPGS01-002_095_083_20100812
LS5_TM_OTH_P51_GALPGS01-002_095_082_20100905
LS5_TM_OTH_P51_GALPGS01-002_095_083_20100905
LS7_ETM_SYS_P31_GALPGS01-002_095_082_20100913
LS7_ETM_SYS_P31_GALPGS01-002_095_083_20100913
LS5_TM_OTH_P51_GALPGS01-002_095_082_20101007
LS5_TM_OTH_P51_GALPGS01-002_095_083_20101007
LS7_ETM_SYS_P31_GALPGS01-002_095_082_20101015
LS7_ETM_SYS_P31_GALPGS01-002_095_083_20101015
LS5_TM_SYS_P31_GALPGS01-002_095_083_20101023
LS7_ETM_SYS_P31_GALPGS01-002_095_082_20101031
LS7_ETM_SYS_P31_GALPGS01-002_095_083_20101031
LS5_TM_SYS_P31_GALPGS01-002_095_082_20101108
LS5_TM_OTH_P51_GALPGS01-002_095_083_20101108
LS5_TM_OTH_P51_GALPGS01-002_095_082_20101023
LS5_TM_OTH_P51_GALPGS01-002_095_082_20101124
LS5_TM_OTH_P51_GALPGS01-002_095_083_20101124
LS5_TM_OTH_P51_GALPGS01-002_095_082_20101210
LS5_TM_OTH_P51_GALPGS01-002_095_083_20101210
LS5_TM_OTH_P51_GALPGS01-002_095_082_20101226
LS5_TM_OTH_P51_GALPGS01-002_095_083_20101226

8.0 Glossary

Item	Description
NBAR	Nadir BRDF (Bi-directional Reflectance Distribution Function) Adjusted Reflectance
TOAR	Top Of Atomosphere Reflectance
DEM	Digital Elevation Model
LS5 TM	Landsat 5 Thematic Mapper
LS7 ETM	Landsat 7 Enhanced Thematic Mapper Plus
ACCA	Automated Cloud Cover Assessment
RGB	Red Green Blue
NDVI	Normalised Difference Vegetation Index
b1, b2	band 1, band 2 etc
UTM	Universal Transverse Mercator
NIR	Near Infrared
3D	Three Dimensional